UNIVERSITY OF CALIFORNIA,
IRVINE

A narrow microtunnel neural network for isolation and precision timing of axon action potentials

THESIS

submitted in partial satisfaction of the requirements
for the degree of

MASTER OF SCIENCE

in Biomedical Engineering

by

Udit Narula

Thesis Committee:
Assistant Professor Beth Lopour, Chair
Assistant Professor Michelle Digman
Adjunct Professor Gregory Brewer

2016

DEDICATION

To my family for their unconditional support,

To Ujjal, Rachana and Prabhjot for their unconditional love,

To Dweep, Sai, Darshik, Vikram for their unconditional friendship.

TABLE OF CONTENTS

LIST OF FIGURES V

ACKNOWLEDGMENTS VI

ABSTRACT VII

1. INTRODUCTION 1

2. METHODS 8

2.1 Fabrication of microtunnel devices 8

2.2 Cell Culture 10

2.3 Recording and spike analysis 12

2.4 Tunnel Imaging 13

3. RESULTS 16

3.1 Spike height and width variation in terms of clusters 16

3.2 Number of clusters per tunnel and their properties 18

3.3 Better segregation of tight clusters in 2.5 μm tunnels from diffuse clusters in 5 and 10 μm wide tunnels 19

3.4 No difference in conduction velocities with tunnel width 21

3.5 Lower axon count in narrow tunnels by confocal microscopy 21

4. DISCUSSION 23

REFERENCES 26

APPENDEX 28

LIST OF FIGURES

Figure 1. Problems of a complex spike. 6

Figure 2. Microtunnel and MEA assembly with burst examples. 9

Figure 3. Tighter clusters of spike waveforms in narrow 2.5 μm compared to 10 μm wide tunnels. 17

Figure 4. Cluster number independent of tunnel width, but cluster tightness strongly influenced by tunnel width. 19

Figure 5. Determination of cluster attributes for different widths. 20

Figure 6. Confocal imaging shows lower axon count in narrow tunnels. 22

ACKNOWLEDGMENTS

I would like to thank my committee members for their valuable time to review my thesis. Professor Beth Lopour, thank you for teaching me valuable lessons in the field of sensory and motor systems. Professor Michelle Digman, thank you for teaching me and being one of the nicest people in Natural Science II. Professor Gregory Brewer, words can't explain how thankful I am to you. From understanding statistics, your lectures, our arguments, and finishing our research paper, I have learned a lot from you during these two years.

I also thank Brendon Cheng for initiating this project and designing the masks for the device molds. I thank Sheng Po (University of Florida) for manufacture of the SU-8 mold to create the PDMS devices and our collaborators Dr. Bruce Wheeler (University of California San Diego) and Dr. Thomas DeMarse (University of Florida) for helpful discussions.

ABSTRACT OF THE THESIS

A narrow microtunnel neural network for isolation and precision timing of axon action potentials

By

Udit Narula

Master of Science in Biomedical Engineering

University of California, Irvine, 2016

Assistant Professor Beth Lopour, Chair

Communication between different sub regions of the hippocampus is fundamental to learning and memory. However accurate knowledge about information transfer between sub regions in individual axons is lacking. MEMS devices with microtunnels connecting two sub networks have begun to approach this problem but common 10 μm wide tunnels frequently produce ambiguous interfering spikes from multiple axons. To reduce this complexity, we compared polydimethylsiloxane (PDMS) microtunnel devices each with a separate tunnel width of 2.5, 5 or 10 μm bridging two wells aligned over a multi electrode array (MEA). After 2-3 weeks of culturing primary rat neurons, with dentate gyrus on one side and hippocampal CA3 on the other of the chamber, spontaneous activity in the axons inside the tunnels was recorded. We report electrophysiological, exploratory data analysis for feature clustering and visual evidence to support our expectation that compared to 10 μm wide tunnels, 2.5 μm wide tunnels have fewer axons per tunnel. Clustering measures comparing the variations of spike height and width for different tunnel widths revealed tighter clusters of spikes with less height and width variation for narrow tunnels. Wider

tunnels tended toward more diffuse clusters from a continuum of spike heights and widths. Standard deviations for multiple cluster measures, such as Average Dissimilarity, Silhouette Value Derivative (S) and Separation Factor, support a conclusion that 2.5 μm wide tunnels with fewer axons enable more precise determinations of individual action potential peaks, their propagation direction and hence timing of information transfer between sub networks.

1. INTRODUCTION

The mammalian hippocampus plays an important role in the formation of long-term episodic memories and spatial navigation, yet encoding in sub-region for different elements of memory formation remains poorly understood. A better understanding of connectivity between different sub regions could aid novel computer designs, improve brain-computer interfaces and new approaches to restoring damaged brain circuits. A mature hippocampus contains three distinguishable subpopulations of neurons: pyramidal cells, granular cells, and interneurons. Each region of the hippocampus (eg. CA1, CA3, DG) exhibits different gene expression profiles [1]. Electrophysiological and immunohistochemical studies of mature hippocampal neurons *in situ* and in slice preparations have revealed that the pyramidal and granular cells are excitatory while the interneurons are inhibitory [2]. Both types of signals contribute to fast synaptic transmission and control of runaway excitation. This phenomenon is considered to be a cellular correlate of learning.

Cortical structure has such a complex nature that it creates a challenge for interpreting single-unit neural activity. Nerve cells in the brain are surrounded by neuroglial cells. From counts of cell nuclei, it has been estimated that they are in equal abundance of glia and neurons [3]. Neurons and glial cells are separated from each other by narrow, fluid-filled, extracellular spaces about 20 nm wide. These spaces provide the least restrictive pathways for extracellular current flow. Accordingly, the challenge in understanding and interpreting *in vivo* neural recordings is complicated by the inhomogeneity of the tissue and by the effects caused by the presence of the microprobe in this environment [4]

The highly ordered arrangement of neurons in such regions of the hippocampus has facilitated *in vivo* studies on cellular physiology, but it has proven difficult to probe collective properties of networks of neurons *in vivo* [5]. One approach is the Utah Intracortical Electrode Array (UIEA) of 100 penetrating silicon microelectrodes designed to focally electrically stimulate or record neurons residing in a single layer up to 1.5 mm beneath the surface of the cerebral cortex [6]. In their studies, Rousche et al. demonstrated that implanted UIEAs were continuously encapsulated at the time of implant, destructively encapsulating the electrodes with fibrous tissue and separating the array from neuron activity. Although the array functioned properly over the chronic implant periods studied, the location of the electrode tips constantly changed as the fibrous tissue accumulated between the array and the cortex. Due to the continuous movement, Rousche et al. could not reliably record the same neuron activity for more than a few weeks on any given electrode.

In another study, Drake et al. [4] used multisite microprobes, fabricated using solid-state process technology, to investigate the closely-spaced columnar organization of cortical tissue. Thin-film multisite microprobes have been under development for over 20 years, but until recently the technology for batch fabricating the supporting substrate did not permit the needed yield or reproducibility. Drake et al. developed a method to batch fabricate microprobes (over 2000 microprobes per 4 in silicon wafer) with greater than 80 percent yield and provide dimensional control to ± 1 μm on structures of arbitrary two-dimensional shape. Different types of Michigan Probes can be used, which have silicon substrate shanks with typical measurements of 15 μm thick, 3 mm long, and 90 μm wide at the base, narrowing to 20 μm at the tip. On the silicon substrates, multiple recording sites

were precisely located and were in configurations having site spacing ranging from 30 to 200 μm. The microprobe is useful for exploring the details of extracellular fields around an active neuron. Results from this research suggest that the neural tissue forms a "tight" seal around the microprobe, permitting closely-spaced recording sites to isolate and explore single-unit extracellular field potentials [4]. This "tight" seal also explains why neural activity can be recorded from several positions on the microprobe shank.

Simultaneous assessment of all the connections of each neuron is not possible with current technology, as each human individual hippocampal neuron averages 100,000 connections [7]. Thus, simultaneous assessment of all the connections of each neuron is not possible with current technology. Patterned substrates have been constructed to better control the connectivity of the network and to explore how geometric connectivity influences computational function. Considerable progress has been made using photoresist, laser, and microstamping techniques for patterning the chemical nature of a substrate, attempting to isolate very small numbers of neurons over a multi electrode array for accurate spike detection [8, 9].

Micro tunnel technology provides highly restrictive paths for connecting axons between different sub networks. The first work in this area was done by [10] involving 3 chambers and a scratched collagen surface for guiding axon growth between primary cultures of sympathetic neurons. Similar designs to channel cortical and hippocampal neurons failed to promote visual axon penetration [11]. In order to address this problem, a transparent PDMS design was produced, with a minimum of two compartments connected to each other through 10 μm wide tunnels, while maintaining fluidic integrity [12]. The electrophysiological activity inside the tunnels can be measured by a multi electrode array (MEA), integrated below the microtunnel devices [11]. Tunnel widths have not been

systematically varied to improve detection performance. As the width of a tunnel decreases, resistance increases, which causes an increase in the spike amplitude [13]. This construct allows simultaneous recordings with μm spatial and μs temporal resolution from a network of axons communicating between two sub regions. Thus, the flow of information between these sub regions through the microtunnels allows precise knowledge of the essential output from one region as the input to the next. Key features of the information transfer are spike direction of propagation from the timing difference on the two electrodes spaced 200 μm apart in the same tunnel and spike and burst dynamics to decode the information transfer. These advantages are predicated on well-isolated spikes.

Compared to open well recording of somal potentials that generally overwhelm the low current source density of axons in a medium of 0.015 MOhm resistance, the increased resistance of 9.6 MOhm inside the 10 μm tunnels increases the signal amplitude from 12 to 200 μV, which readily allows precise detection of axon action potentials [14]. However, multiple axons in each 10 μm wide tunnel still creates problems of attribution of axon identity due to complex spikes. Fig 1A shows the features of a complex spike with smaller spike amplitude and larger width, due to constructive and destructive interference caused by the simultaneous detection of action potentials from two axons in the same tunnel. To demonstrate the principle of the problem, a spike overlapping model was created (Fig 1C), which shows how two axons over one electrode could generate two spikes, moving in different speeds (0.4 and 0.5 m/s respectively). The constructive and destructive interference of these spikes with different frequencies, create sorting problems when waveforms overlap that could be precluded if more narrow tunnels could restrict tunnel occupancy to single or a reduced number of axons with clean distinction of the waveforms.

Here, we propose to reduce the number of axons passing over the electrodes in tunnels to improve precision in the μs timing information spikes passing between two sub networks. We wanted to test whether tunnels of a narrower width of 5 or 2.5 μm would maximize the detection of well-isolated spikes within more restricted clusters of height and width types. This would allow us to more accurately measure directionality from the timing of spikes from single axons passing over electrodes spaced 200 μm apart and improve the accuracy of the spike timing dynamics. Relationships of network communication require knowledge of timing directions in inter-network communication, which is also achieved by axon isolation. To provide confidence of better axon isolation, a novel clustering approach was used to determine the relationship between tunnel width and the variation of spike height and width. In this paper, we report electrophysiological, exploratory data analysis for feature clustering and visual evidence to show that narrower tunnels of 2.5 μm allow passage of fewer axons per tunnel with less ambiguous assignments of peak times in comparison to wider tunnels of 5 or 10 μm.

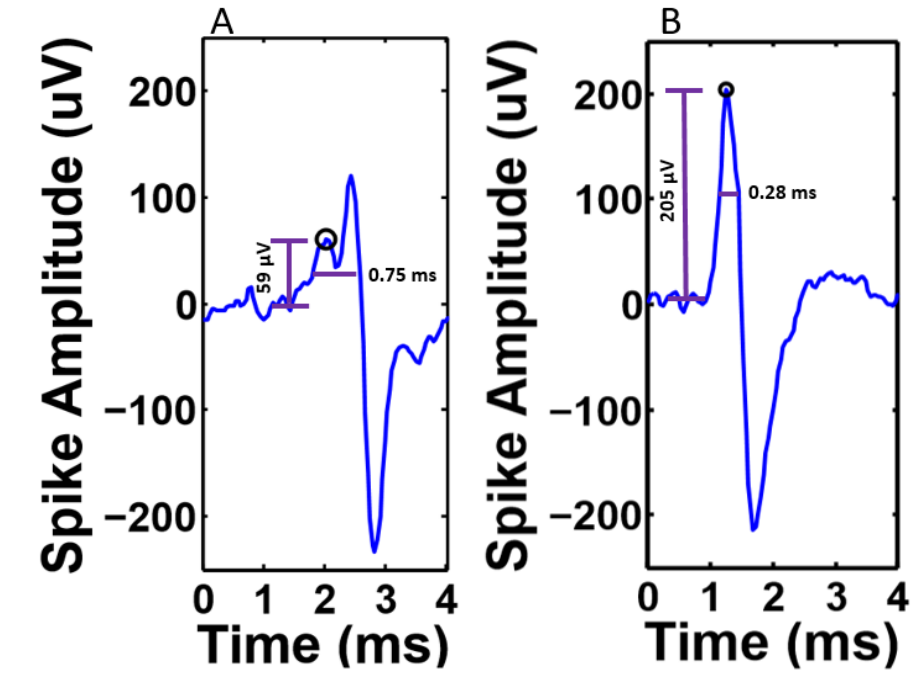
A
B
Spike Amplitude (uV)
Time (ms)
59 µV
0.75 ms
205 µV
0.28 ms

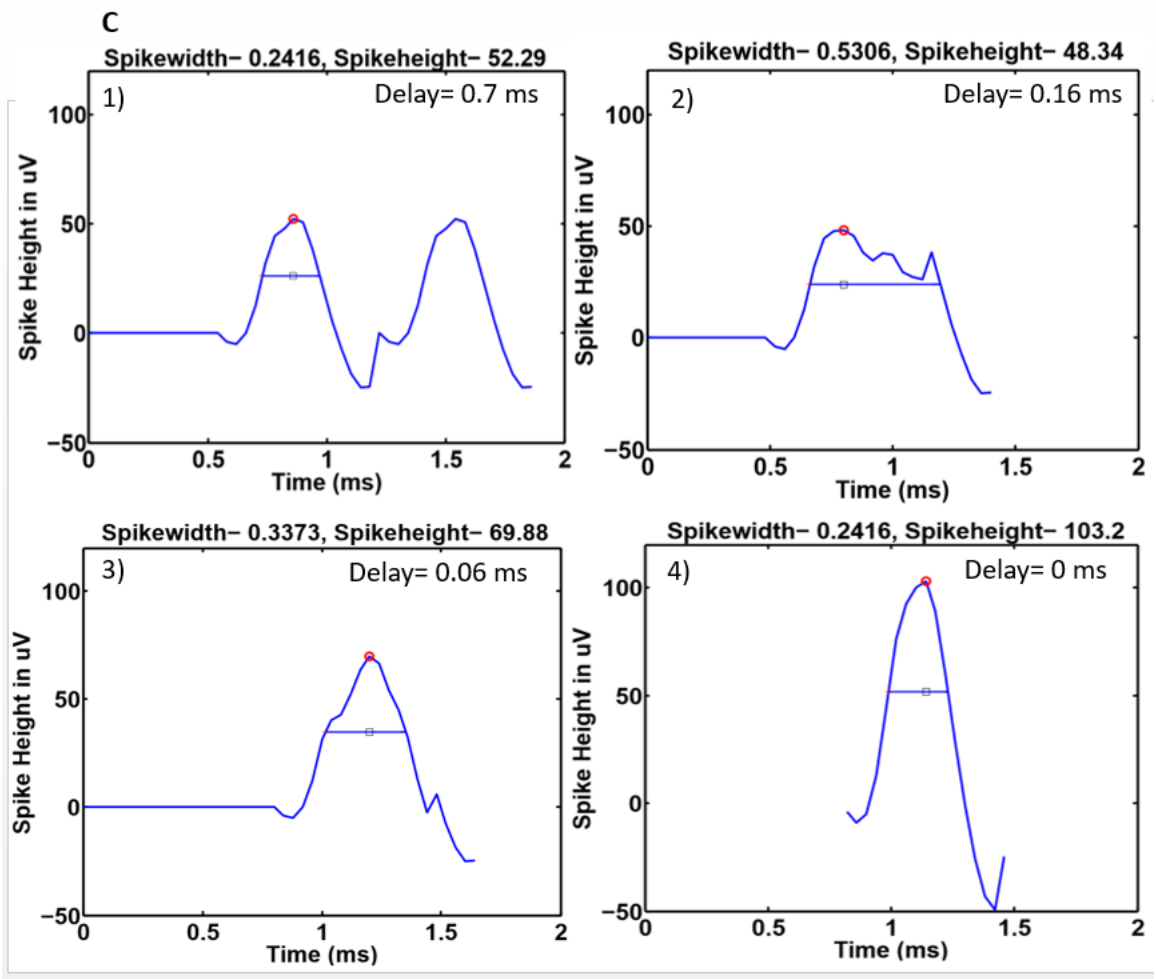
C
Spikewidth− 0.2416, Spikeheight− 52.29
1)
Delay= 0.7 ms
Spikewidth− 0.5306, Spikeheight− 48.34
2)
Delay= 0.16 ms
Spikewidth− 0.3373, Spikeheight− 69.88
3)
Delay= 0.06 ms
Spikewidth− 0.2416, Spikeheight− 103.2
4)
Delay= 0 ms
Spike Height in uV
Time (ms)

Fig 1. Problems of a complex spike (A) commonly observed in 10 μm tunnels with smaller height (32 μV) and larger width at half-height (0.75 ms) due to constructive and destructive interference from the collision of two action potentials recorded by the same electrode. Note the detection of a subcomponent of the complex spike with low but sufficient amplitude (circle) at a local maximum that exceeds 9x the noise and subsequent failure to detect the larger amplitude maximum because of the 1.6 ms dead time imposed. (B) Accurate detection of timing of a clean spike with larger height (114 μV) and smaller width (0.2 ms) also from a 10 μm wide tunnel. We investigated whether narrower tunnels would favor increased detection of clean spikes and decrease complex spikes. (C) Spike overlapping model of a 10 and an 11 Hz waveform. Note, when the waveforms are 0.16 ms apart, the spike height is decreased and the width is increased due to collisions, whereas when the waveforms are aligned over each other (0 ms apart), spike height is increased and width is decreased.

2. METHODS

2.1 Fabrication of microtunnel devices

All tunnels were 800 μm long to preclude edge alignment problems, but they were truncated at 400 μm long by the separation of two compartments (Fig. 2). The devices were designed for the use with MEAs from MCS (Multi Channel Systems, Reutlingen, Germany), which have 30 μm diameter electrodes with 200 μm inter-electrode spacing. The mold fabrication process comprises the formation of two layers of SU-8: a first thin structure of the microtunnels and a second thick structure for forming the culture wells, very similar to our earlier report [14]. We reordered the fabrication steps to permit alignment of the culture well mask to the microtunnel mold structures. Briefly, a standard 4-inch, single-side polished silicon wafer was cleaned by piranha solution (H_2SO_4: H_2O_2 = 3:1) for 15 min, then treated on a hotplate. Photoresist SU-8 2002 (Microchem, Westborough, MA) was spun on at a nominal thickness of 2.5 μm. For maximum resolution, the SU-8 was exposed through the backside a chromium on glass microtunnel mask (Photo Science Inc., Torrance CA) post-exposure baked and developed. After fabrication of the microtunnels, SU-8 2050 (Microchem) was poured on the substrate to a thickness of 1 mm. Then the wafer was soft-baked, exposed with the microwell mask (CAD/Art Services Inc., Bandon, OR), post-exposure baked and developed.

In order to facilitate release of PDMS devices from the molds, the mold was silanized in a desiccator in the presence of 20 μL 2-Methoxy(Polyethyleneoxy propyl)trimethoxysilane (Gelest, San Diego, CA), overnight. PDMS along with curing agent (Dow Corning, Bay City, MI) in 10:1 ratio was poured over the whole wafer surface inside an aluminum foil boat. After removing bubbles in a vacuum chamber, a 0.05 mm thick layer of PET plastic was

pressed onto the PDMS over the wafer and about 50 gm of weights applied, so as to rest on the tops of the chambers. The assembly was placed in a 60°C oven for 45 minutes. After cooling to room temperature, the weights were removed and plastic cover carefully peeled off. A 1 cm hole was punched to release each of 15 devices with tunnels as their center.

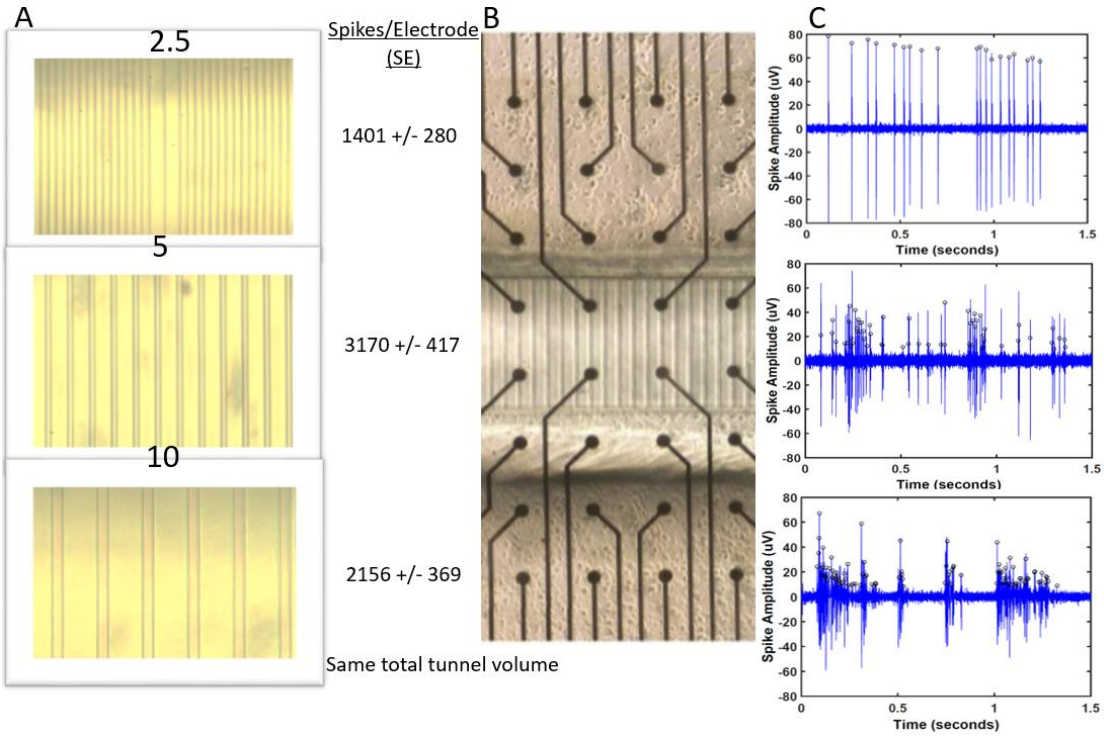

Fig 2. Microtunnel and MEA assembly with burst examples. (A) Tunnel widths 2.5, 5 and 10 µm, with number of tunnels adjusted for equal volume. Mean and S.E. of spikes per electrode are shown. (B) The devices are aligned over 2 middle rows of an MEA (inter-electrode spacing 200 µm). Neurons are seen outside the tunnels, but lighting was optimized here to show tunnels. (C) Bursts in different tunnel widths 2.5, 5 and 10 µm. Note more uniform heights of higher amplitude in the 2.5 µm wide tunnels.

Each device was aligned on an MEA using a mask alignment microscope. The MEA is attached to a metal plate, via vacuum suction, while the device starts on a 15 mm glass cover slip with 10 µL ethanol, just below it as a release layer. In close proximity, the center

two rows of the MEA were aligned over the tunnels. A dark contact pattern was seen on contact, attaching the device to the MEA, perfectly aligning the tunnels to the desired electrodes.

To promote adhesion of the neurons and passage of the axons through the tunnels, poly-D-Lysine in water, 100 μg/ml, was applied, (P6407, Sigma-Aldrich, St. Louis, MO). First we put 6 μL ethanol on one side of the chamber, and then the other side to wet the tunnels and avoid trapping bubbles. Then ethanol from one chamber is aspirated and immediately replaced by PDL and followed by removal of ethanol from the other side to cause the PDL to be pulled through the tunnel by gravity. After 10 minutes, PDL was added to the other chamber. To make sure that ethanol is not present in the chambers, PDL in each chamber is replaced by fresh PDL. The devices were kept covered overnight at room temperature in the sterile hood. The next day, PDL was aspirated, replaced with water and aspirated again. The devices were then left to dry for 3 hours. Once dried, we pipette 6 μL NbActiv4 culture medium (BrainBits, Springfield, Illinois) + Gentamycin (100 μg/ml, (Gibco-ThermoFisher, NY) in one chamber and then the other chamber and place the device in the incubator.

2.2 Cell Culture

Postnatal day 3 Sprague-Dawley rats (Charles Rivers Labs, San Diego) were anesthetized, brains removed and placed into 2 ml Hibernate A/Glx minus calcium (BrainBits) in a 35 mm D dish. The CA3, DG subregions of 3 brains were dissected and transferred to a 15 ml tube filled with Hibernate A – Ca, Glutamax, which is a dipeptide substitute for L-glutamine at 4^{o} C (1 μg/ml, Gibco-ThermoFisher, NY). The tube with tissue, along with a tube filled

with papain (2 mg/ml, BrainBits), were warmed at 30 ^{o}C for 10 minutes. The tissue was then transferred into the papain tube and further incubated for another 10 minutes. The tissue was transferred in 1 ml Hibernate A/B27/Glutamax (BrainBits, Springfield, Illinois) and triturated using a fire polished 9" pipet (BrainBits), until most of the tissue was homogenized. Non-dispersed pieces were allowed to settle for 3 minutes. The supernatant was transferred to a new tube, diluted with 2 ml Hibernate A/B27/Glutamax and centrifuged for 1 minute at 200 G. The supernatant was discarded and the pellet with about 20µl of residual supernatant was not disturbed. The tube was flicked to disperse the cells and diluted with 50µl or 100µl NbActiv4+ gentamycin for DG and CA3, respectively. 10 µl of the concentrated cells were mixed with 10 µl 0.4% trypan blue (Sigma) for counting in a hemocytometer. After the counting, the cells were diluted in order to plate 10,000 cells per well (6,000 cells/mm^2). The devices were removed from the incubator and the medium was aspirated from the two chambers leaving a small amount to keep the tunnels filled. Source DG cells were plated by gently pipetting 7 µl with a repeat action to ensure wetting the tunnel entrance. The devices were kept in the incubator for 10 minutes. After that, CA3 cells were plated in the other chamber, by pipetting gently two times near the tunnel entrance, and incubated for 30 minutes. Once the cells attached, 160 µl warm CO_2-equilibrated NbActiv4 + gentamycin was added. The incubator kept the cells at 37 °C with 9% O_2 and 5% CO_2, balance N_2 in a humidified incubator (Thermo-Forma #3432, Marietta, OH). Evaporation was limited by a teflon sheet covering the MEA (ALA Scientific, Farmingdale, NY). 50% of the medium was changed twice a week with pre-equilibrated medium.

2.3 Recording and spike analysis

Multi Electrode Arrays (MEA) from Multi Channel Systems (Reutlingen, Germany) with 60 TiN_3 electrodes, one being ground, 30 μm in diameter and 200 μm apart. Signals were amplified at a gain of 1200x, sampling rate of 25 KHz, at 37 ^oC, under sterile flow of 5% CO_2, 9% O_2, balance N_2 (Airgas, Palmdale, CA). Spontaneous activity in the networks was recorded for 5 min. after 2-3 weeks of culture. Data analysis was performed by using SpyCode v3.9 [15] along with multiple MATLAB scripts (The MathWorks, Inc, Natick, Massachusetts). The central 2 rows of the MEA were selected for analysis, filtered at 300 Hz high pass, and identified as peak to peak amplitude that exceeded 9 times the root mean square of a 200 ms contiguous window. A refractory period of 1.6 ms was used. Threshold level was set for each electrode via the Graphical User Interface of SpyCode. SpyCode efficiently gives spike timing at the peak, but spike height and spike width were determined by custom MATLAB scripts. Out of all the spikes detected, only the positive arm of each spike was analyzed with amplitude defined as the distance from 0 μV to the positive peak of spike. Spike widths were calculated at half height of the positive arm. To analyze the effect of tunnel width on log10 values of spike height and width variation, a clustering approach was implemented. To determine the number of clusters present in each tunnel, three people inspected each spike height by width scatter plots (blinded to tunnel width). Based on the predominant cluster number, MATLAB Kmedoid function and custom scripts were used to characterize clusters. This analysis not only analyzed spike height and width variations in individual clusters, but also the separation of the clusters. Plots of height against width revealed tighter clusters with less variation in spike height and width, whereas diffuse clusters arose from higher variation. A quantitative measure of each

cluster was determined as average dissimilarity (average of sum of all the distances from each point to the medoid in their respective clusters). Another measure was the Silhouette Value Derivative (S) of how similar an object is to its own cluster compared to other clusters. A third measure was Separation Factor (average dissimilarity divided by S value). The variability of each of these measures was computed as the standard deviation of spike width and height. Spike velocity was calculated by dividing the distance between two electrodes (200 μm) in a tunnel by the difference in spike times. Velocities from 0.2 – 0.83 m/s were considered as paired spikes; spikes under 0.2 m/s were considered ambiguous due to likely detection of spikes from two axons. Velocities above 0.83 m/s are termed as unpaired. [16]

Average Dissimilarity= ai Silhouette Value= (bi-ai)/ max (ai, bi), where bi is the minimum average distance from the medoid to points in a different cluster. Separation Factor= Average Dissimilarity/Silhouette Value

2.4 Axon Tracing and Tunnel Imaging

Neurons are composed of a cell body, dendrites and an axon. Axons transmit impulses to other neurons or effector cells. Besides impulse conduction, another important axon function includes transport of materials from the soma to the axon terminals for synaptic communication to the next neuron. This direction is anterograde transport to the axon terminal; in retrograde transport, the direction is from the axon terminal to the cell body [17]. Neuronal tracing allows for precise identification of neuronal pathways and functions. The anterograde and retrograde tracing techniques allow for detailed descriptions of

neuronal projections from a single population of neurons to their various targets throughout a network.

Axons transport a variety of substances. Anterograde transport is used in the translocation of membranous organelles and vesicles as well as of macromolecules, such as actin, myosin, and clathrin, and some of the enzymes necessary for neurotransmitter synthesis at the axon terminals mediated by the kinesin family of proteins [17]. Retrograde transport returns items to the cell body from the axon. This includes protein building blocks of neuroflaments, subunits of microtubules, soluble enzymes and materials taken up by endocytosis mediated by cytoplasmic dyneins. Axonal transport can be combined with immunocytochemistry for the neurochemical characterization of specific neuronal pathways.

The axon growth cones are able enter inside and extend to traverse the entire 400 μm length of the microtunnels that we created, whereas their cell body remains outside. Therefore we used Calcein-AM for anterograde staining of the cytoplasm. The AM (acetoxymethylester)-form of the fluorescent probe is non-fluorescent but cell permeable. Once inside a cell, non-specific esterases cleave the AM to release the green fluorescent calcein that diffuses throughout the cytoplasm.

The microtunnel devices were attached to 15 mm glass cover slips (German glass, 0.22 mm, Fisher Scientific), coated with PDL. The cells were grown in the two chambers in the same way as in the devices on MEAs. Imaging of axons inside the tunnels was facilitated by replacing the medium in the chamber containing the DG sub region with 2 μl Calcein AM (Thermo Fisher Scientific, Carlsbad, CA, diluted to 1 μg/500 μl NbActiv4). After an incubation of 20 min at 37 ^{o}C in the CO_2 incubator, the chamber with DG was rinsed with

Hibernate A LF/glx at 37 ^{o}C (BrainBits) and then the whole device with Hibernate A LF/glx. Axons were imaged by confocal microscopy (LSM 510 Zeiss, Munich, Germany) at 60x magnification with a 488 nm argon laser with a scan time of 4 seconds. The images were obtained with an optimum z-slice interval of 0.1 μm. A stack of 6 images was used to create an image containing small standard deviation of the intensities at each pixel, which eliminates noisy pixels by using ImageJ v1.63r [18]

3. RESULTS

3.1 Spike height and width variation in terms of clusters

To determine whether narrow tunnels produced a higher yield of isolated action potentials from fewer axons, we used the k-medoid function of MATLAB to sort and classify spike width and height characteristics. We assumed that a single axon in one tunnel would produce spikes of similar heights (and widths) and tightly cluster these features within a narrow range, different from a tight cluster of features for axons in other narrow tunnels and different from a more diffuse cluster in wider channels. To validate the clustering algorithm based on spike height and width features, we examined the waveforms for each cluster. Fig 3A shows a cluster plot for a 2.5 μm tunnel with a worst case of four clusters. Waveforms for each cluster (B-E), aligned well over each other (first 100 spikes shown). The near perfect overlap of waveforms suggests that tightness of a cluster can be linked with consistency in spike height and width. Fig 3F shows a cluster plot for a 10 μm tunnel with one diffuse cluster. Waveforms for the diffuse cluster (G) are poorly aligned forming a continuum over a large range of spike heights and widths. We call this a diffuse cluster. If the same diffuse cluster is forced into 3 clusters (H), the wide continuum of heights and widths is more readily evident (I-K) in especially when recombined (L). With this better understanding of extreme examples of tight and diffuse clustering, we could next determine whether they were statistically associated with narrow and wide tunnels.

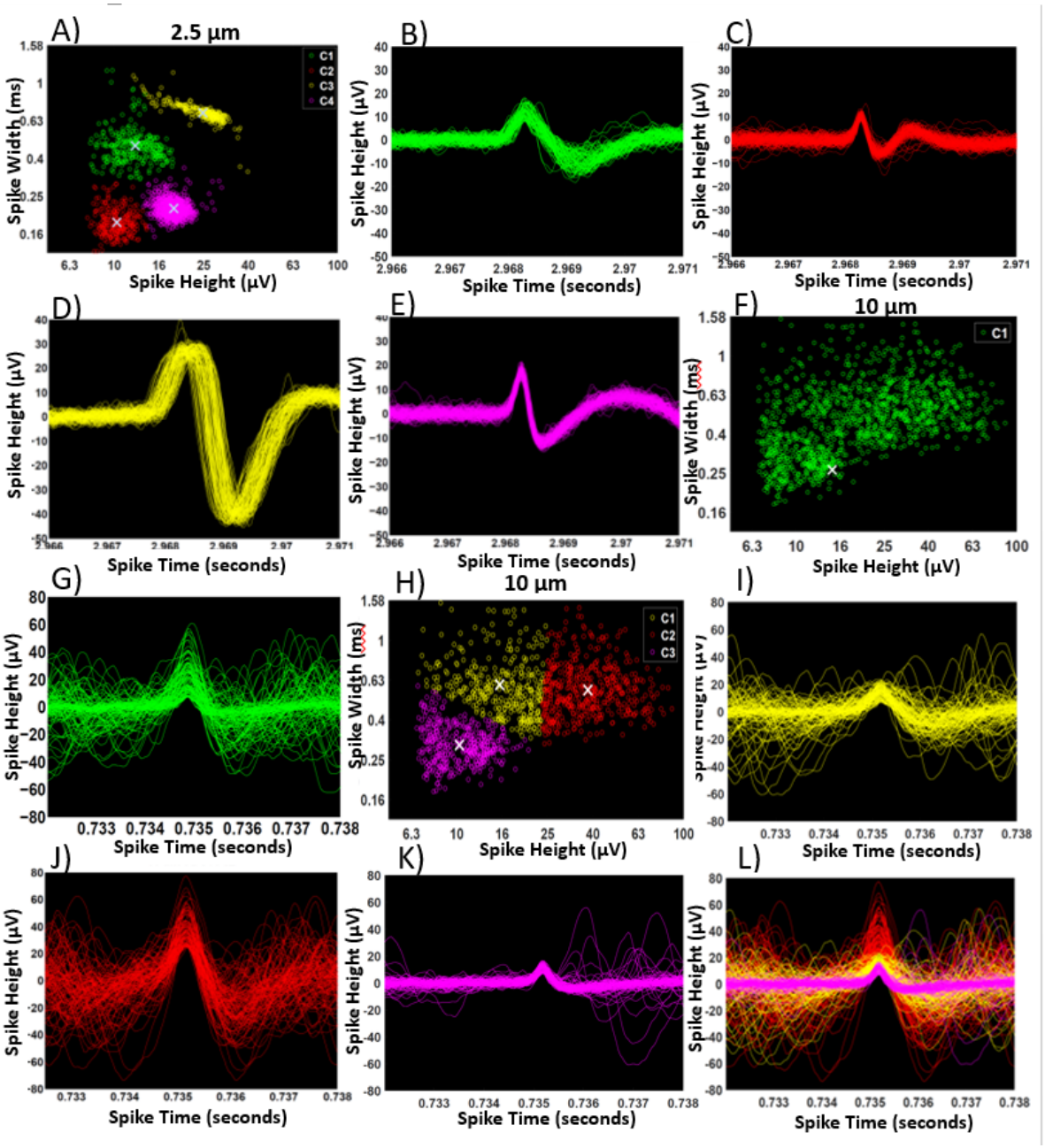

Fig 3. Tighter clusters of spike waveforms in narrow 2.5 µm compared to 10 µm wide tunnels. (A) 2.5 µm wide tunnel with tight clusters. X marks the medoid of each cluster. Tight alignment of the waveforms (B-E) of the first 100 spikes shown for clarity (total spikes in each cluster: C1- 313, C2- 271, C3- 278, C4- 1138). (F) 10 µm tunnel of a diffuse cluster. First 100 spikes out of 2212 are shown in (G), which are aligned poorly. Forced clustering (H) of data from (F) failed to show discrete waveforms in first 100 waveforms of each cluster (I, J and K). Note that the composite (L) produced a continuum of waveform heights and widths.

3.2 Number of clusters per tunnel and their properties

We tested whether narrow tunnels would exhibit fewer clusters from less axons per tunnel than the wide tunnels. Fig 4A shows that one cluster per 2.5 μm wide tunnel was most prevalent, although by no means exclusive (mean 2.4 ± 0.3 clusters per tunnel). For 5 μm wide tunnels, 2 or 3 clusters were most prevalent (mean 2.4 ± 0.1). Surprisingly, single clusters were nearly as prevalent in 10 μm wide tunnels as in 2.5 μm wide tunnels, although 2 clusters were also common (mean 1.9 ± 0.2). The mean cluster count was insignificantly different ($F(2,86)=2.13$, $p=0.125$). From Fig 3F, we considered whether a single diffuse cluster could arise from constructive and destructive interference of multiple action potentials from multiple axons, which would compromise the precision of spike timing (Fig3 F-L). To observe whether tunnel width affected the tightness or diffuseness of the action potentials widths and heights, we determined the distribution of dissimilarity measures from each tunnel. Dissimilarity is the sum of all the distances from each point to the medoid in each cluster divided by the number of spikes. Fig 4B shows this distribution of dissimilarities per tunnel with 2.5 μm tunnels having 50 % higher number of tight clusters than wider tunnels (5 and 10 μm). Conversely, 5 and 10 μm wide tunnels produced more diffuse clusters. For the 38% of single clusters in 10 μm wide tunnels, the average dissimilarity was 0.07 ±0.01, indicating the diffuse type, compared to 0.04 ±0.01 for the 41% of single clusters in 2.5 μm wide tunnels, indicating a tight cluster type (Fig 4C). These results suggest that 2.5 μm tunnels have more single tight clusters than wider tunnels and the single clusters seen in 10 μm wide tunnels were more often diffuse.

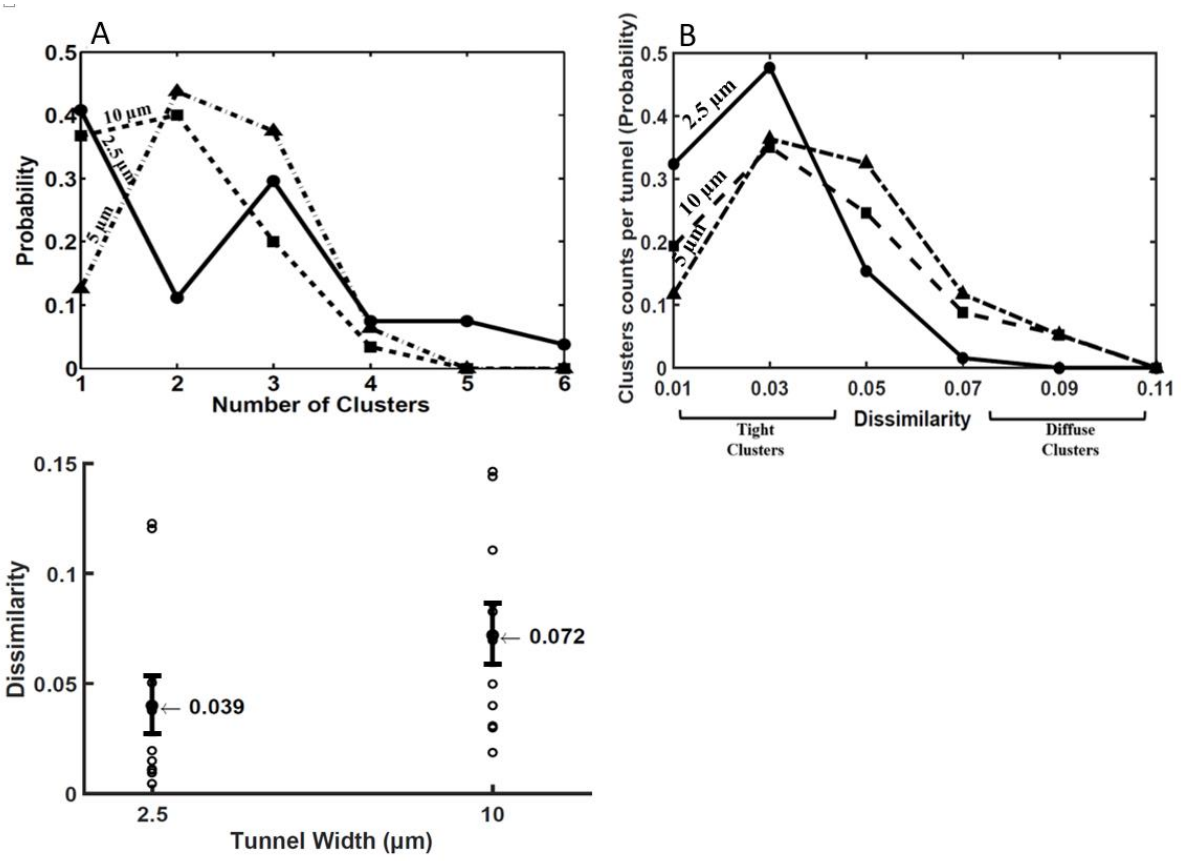

Fig 4. Cluster number independent of tunnel width, but cluster tightness strongly influenced by tunnel width. (A) Distribution of clusters per tunnel for 2.5, 5 and 10 µm tunnels. (B) Distribution of dissimilarity measure of cluster tightness or diffuseness. (C) Dissimilarity measure for single clusters in 2.5 and 10 µm tunnels.

3.3 Better segregation of tight clusters in 2.5 µm tunnels from diffuse clusters in 5 and 10 µm wide tunnels

To determine the consistency of the spikes in each cluster, we computed the Average Dissimilarity (AD). AD is the sum of all the distances from each point to the medoid in their respective clusters divided by the number of points. It represents how tight or diffuse a cluster is for individual clusters only. Fig 5A shows that spike clusters were significantly tighter (more consistency in spike height and width) for 2.5 µm tunnels than wider tunnels. The silhouette metric determines how similar an object is to its own cluster compared to

other clusters, and is a common method to measure cluster attributes. To better adjust for cases when we have just one cluster, a new method of separation factor (SF) was derived, SF is the ratio of average dissimilarity and silhouette value of respective clusters. The silhouette value for one cluster is set at 1, for best separation, as there is only one cluster. Evaluation of separation factor (Fig 5B) also shows a significant decrease in value in 2.5 μm tunnels compared to wider tunnels, suggesting the presence of better separation of axon spike times. The distribution of the clusters of spike types (Fig 5C) showed a clear shift to tighter, lower standard deviations from the medoid compared to 5 and 10 μm tunnels. Further, fig 5D shows that 2.5 μm tunnels exhibit a lower Standard Deviation (SD) of each cluster for distance of each spike height and width from the medoid than wider widths, more evidence for tighter clusters in 2.5 μm wide tunnels.

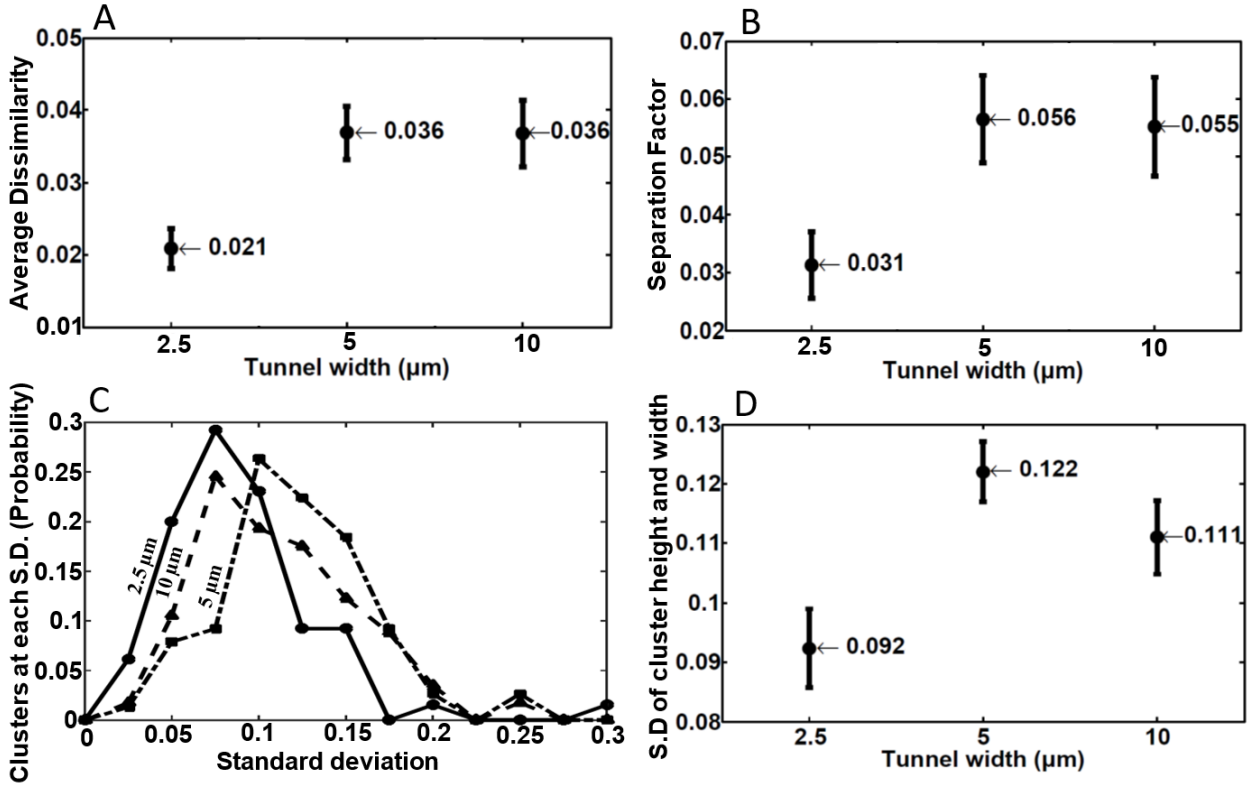

Fig 5. Determination of cluster attributes for different widths. (A) Average dissimilarity between the observations in the cluster and the cluster's medoid, $F(2,196)=6.2$, $p=0.002$. (B) Separation Factor is the ratio of average dissimilarity and silhouette value, $F(2,86)=3.41$, $p=0.037$. (C) Distribution of the clusters at each standard deviation for different tunnel widths. (D) Standard Deviation of cluster's spike widths and heights per tunnel width, $F(2,195)=6.79$, $p=0.001$.

3.4 No difference in conduction velocities with tunnel width

Because we have 2 electrodes in each tunnel, we can measure the velocity of propagation of the action potentials for the predominant direction. Directional propagation from DG to CA3 was a similar 64 % of the total paired spikes from 2.5 and 10 μm tunnels, in agreement with previous results in 10 μm wide tunnels [16]. From 2.5, 5 and 10 μm tunnels, we detected insignificantly different average speeds of 0.43 ± 0.04, 0.48 ± 0.05 and 0.38 ± 0.02 m/s respectively in the predominant direction (DG->CA3) ($F(2,46)=2.05$, $p=0.14$), suggesting that the axon diameter is similar in each tunnel width. The observed speeds are consistent with the extra-burst measures of 0.54 m/s reported previously [16].

3.5 Lower axon count in narrow tunnels by confocal microscopy

Confocal images were taken from 3 week cultures for visual evidence of fewer axons in narrow tunnels. As seen in the image in Fig 6A, C one or two axons were seen inside 2.5 μm tunnels, whereas in 10 μm tunnels (B), two or more axons are readily resolved (6B, D). This suggests that we were able to reduce the number of axons inside narrow tunnels, but we failed to achieve frequent single axons.

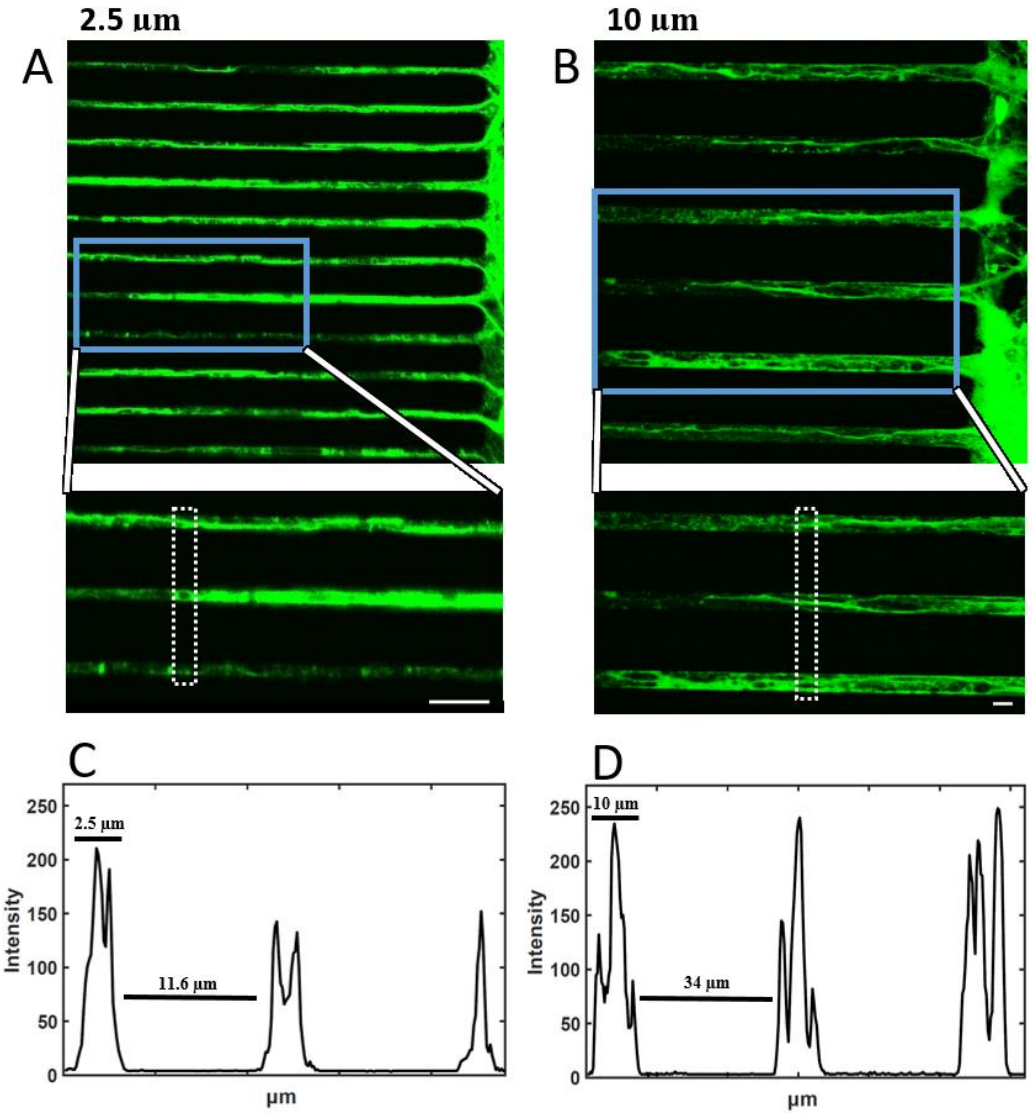

Fig 6: Confocal imaging shows lower axon count in narrow tunnels. (A) 2.5 µm tunnels, (B) 10 µm tunnels shows comparatively higher axon count (average of 3 axons per tunnel). Scale bar=10 µm (A and B). Intensity plots of the blue line over the enlarged area (A and B) are shown in C (2.5 µm) and D (10 µm). Note that narrow tunnels show 2, 2 and 1 axons, whereas 3, 3 and 3 axons can be seen in the 10 µm tunnels.

4. DISCUSSION

Multiple neurons or axons per electrode leads to variations in recorded spike amplitudes and widths contributing to imprecise spike timing. We attempted to solve this problem of resolution by isolation of single axons for greater spike timing precision. For the first time, we created microtunnels with narrow widths of 2.5 and 5 μm to systematically compare to the more common 10 μm wide tunnels. Compared to 10 μm wide tunnels, 2.5 μm wide tunnels exhibited spike heights and widths clustered into groups with smaller average dissimilarity, separation factor and standard deviation. Action potentials from axons in 2.5 μm tunnels were clustered into tighter groups, well segregated and with their waveforms well aligned, in contrast with those in 10 μm wide tunnels which showed much greater variation in spike height and width. Visual evidence of axons inside the tunnels from confocal imaging showed fewer axons in narrow 2.5 μm tunnels than 10 μm wide tunnels, again supporting our hypothesis. However, we were unable to consistently isolate single axons. Hippocampal axon width is approximately 0.8 μm [19], which means that even the narrow tunnel width of 2.5 μm could accommodate up to 9 axons with three in direct contact with the 30 μm electrode. In one case of a 2.5 μm tunnel we observed a maximum of 6 tight clusters, suggesting 6 axons. In the future, we may be able to isolate single axons by reducing the plating density of cells at the expense of unoccupied tunnels and lower network activity. Another approach to isolate single axons would be to decrease the tunnel width to 1 μm, which is achievable with UV-laser light [20]

A major hurdle in understanding learning and memory has been to achieve neuronal networks of different sub regions of neurons with simultaneous access to internetwork/inter-regional communication [21]. Axon-selective microtunnels of 10 μm

width were made to visualize bundles of axons [12, 22] and for analysis of CNS axonal injury and regeneration [23]. Electrical activity of the axons was recorded from a single electrode [24] and multisites [14, 25] through the tunnels with a higher signal-to-noise value [13] than conventional open-access substrate-embedded microelectrodes. As Wang et al. decreased the cross sectional dimensions of tunnels from 3.5 x 25 μm (92 μm^2) to 1 x 5 μm (5 μm^2), the variability in spike height increased but the median height did not significantly increase. We suspect that they failed to demonstrate increased height because they did not examine clusters based on spike height and width, as we did here. Also the SNR for the different dimensions remained insignificantly different, which is consistent with our data (13, 11 and14 for 2.5, 5 and 10 μm tunnels respectively). Spike propagation direction and speed were further examined [16, 26] to better understand the connectivity between different sub regions of the hippocampus in 10 μm wide and now 2.5 μm wide tunnels. None of this previous work has led to isolation of single axons in microtunnels consistently, which we have approached in this paper using narrow tunnels.

Electrical activity of axons within a myelinated fiber would be ephaptically coupled and synchronized [27]. In the case where unmyelinated axons are present, as in microtunnels [26], one could also hypothesize that the membranes of pairs of axons could be even more tightly coupled, near gap junction tightness. In such close proximity, an action potential in one axon induces an action potential in another axon, by ephaptic coupling from highly localized sodium and potassium fluxes. Thus, an action potential in one axon begins with sodium influx, quickly followed by potassium efflux. This first lowers the extracellular sodium and then raises potassium, both of which may partially depolarize a nearby axon. The current loop from one impulse induces a longitudinal voltage,

influencing the dynamics of an adjacent impulse [28]. Further, the change in local ion flux produces only small 0.5 mV changes in adjacent axon potential, insufficient to depolarize. However, together with normal membrane fluctuations, this periodic 0.5 mV change is sufficient to entrain the timing of action potentials of adjacent axons [29]. It is well known that the induced second action potential is delayed by 0.5 ms [30], which is within our measured 0.2-0.8 ms range of spike widths. Hence, an ephaptic spike could cause spike overlap and broadening. This ephaptic coupling would be more likely to occur in narrow 2.5 μm tunnels, where the axons are in closer proximity to each other. Ephaptic coupling in narrow tunnels could induce a faster propagation speed than the regular spike because of higher field amplitude [31], which might explain a larger variation in the observed velocities.

In conclusion, based on analysis of spike waveforms, multiple axons in wider tunnels are more likely to interfere with precise detection of spike timing compared to fewer axons in narrow tunnels. We have been able improve isolation of fewer axons inside the 2.5 μm tunnels compared to the wider microtunnels (10 μm). Our result is supported by electrophysiological tests, exploratory data analysis for feature clustering and visual evidence of the axons inside the microtunnels. Our work will help to decode the information flow between reconstituted brain sub regions, along with drug trials for neurological diseases with higher precision.

REFERENCES

1. Lein ES, Zhao X, Gage FH. Defining a molecular atlas of the hippocampus using DNA microarrays and high-throughput in situ hybridization. The Journal of neuroscience : the official journal of the Society for Neuroscience. 2004;24:3879-89.
2. Stenger DA, Hickman JJ, Bateman KE, Ravenscroft MS, Ma W, Pancrazio JJ, et al. Microlithographic determination of axonal/dendritic polarity in cultured hippocampal neurons. Journal of Neuroscience Methods. 1998;82:167-73.
3. Azevedo FA, Carvalho LR, Grinberg LT, Farfel JM, Ferretti RE, Leite RE, et al. Equal numbers of neuronal and nonneuronal cells make the human brain an isometrically scaled-up primate brain. Journal of Comparative Neurology. 2009;513:532-41.
4. Drake KL, Wise K, Farraye J, Anderson DJ, BeMent SL. Performance of planar multisite microprobes in recording extracellular single-unit intracortical activity. Biomedical Engineering, IEEE Transactions on. 1988;35:719-32.
5. Kleinfeld D, Kahler KH, Hockberger PE. Controlled outgrowth of dissociated neurons on patterned substrates. The Journal of neuroscience : the official journal of the Society for Neuroscience. 1988;8:4098-120.
6. Rousche PJ, Normann RA. Chronic recording capability of the Utah Intracortical Electrode Array in cat sensory cortex. Journal of Neuroscience Methods. 1998;82:1-15.
7. Garenne A, Chauvet P, Daya B, Chauvet G, editors. Dynamic learning model of eyeblink conditioned reflex: Computational simulation and implications. Proc of the IASTED International Conference on Artificial Intelligence and Applications; 2004.
8. Ikurou S, Yoshihiro S, Yasuhiko J, Kenji Y. Individual-Cell-Based Electrophysiological Measurement of a Topographically Controlled Neuronal Network Pattern Using Agarose Architecture with a Multi-Electrode Array. Japanese Journal of Applied Physics. 2004;43:L403.
9. Suzuki I, Sugio Y, Jimbo Y, Yasuda K. Stepwise pattern modification of neuronal network in photo-thermally-etched agarose architecture on multi-electrode array chip for individual-cell-based electrophysiological measurement. Lab on a chip. 2005;5:241-7.
10. Campenot RB. Local control of neurite development by nerve growth factor. Proc Natl Acad Sci U S A. 1977;74:4516-9.
11. Jeon NL, Cotman C, Taylor AM. Microfluidic device for enabling fluidic isolation among interconnected compartments within the apparatus and methods relating to same. Google Patents; 2008.
12. Rhee SW, Taylor AM, Tu CH, Cribbs DH, Cotman CW, Jeon NL. Patterned cell culture inside microfluidic devices. Lab on a chip. 2005;5:102-7.
13. Wang L, Riss M, Buitrago JO, Claverol-Tinture E. Biophysics of microchannel-enabled neuron-electrode interfaces. J neural eng. 2012;9:026010.
14. Dworak BJ, Wheeler BC. Novel MEA platform with PDMS microtunnels enables the detection of action potential propagation from isolated axons in culture. Lab on a chip. 2009;9:404-10.
15. Bologna LL, Pasquale V, Garofalo M, Gandolfo M, Baljon PL, Maccione A, et al. Investigating neuronal activity by SPYCODE multi-channel data analyzer. Neural Networks. 2010;23:685-97.
16. Brewer GJ, Boehler MD, Leondopulos S, Pan L, Alagapan S, DeMarse TB, et al. Toward a self-wired active reconstruction of the hippocampal trisynaptic loop: DG-CA3. Frontiers in neural circuits. 2013;7:165.
17. Oztas E. Neuronal tracing. Neuroanatomy. 2003;2.
18. Schneider CA, Rasband WS, Eliceiri KW. NIH Image to ImageJ: 25 years of image analysis. Nature methods. 2012;9:671-5.

19. Bartlett WP, Banker GA. An electron microscopic study of the development of axons and dendrites by hippocampal neurons in culture. I. Cells which develop without intercellular contacts. The Journal of neuroscience : the official journal of the Society for Neuroscience. 1984;4:1944-53.
20. Ghosh S, Ananthasuresh GK. Single-photon-multi-layer-interference lithography for high-aspect-ratio and three-dimensional SU-8 micro-/nanostructures. Scientific Reports. 2016;6:18428.
21. Berdondini L, Chiappalone M, van der Wal PD, Imfeld K, de Rooij NF, Koudelka-Hep M, et al. A microelectrode array (MEA) integrated with clustering structures for investigating in vitro neurodynamics in confined interconnected sub-populations of neurons. Sensors and Actuators B: Chemical. 2006;114:530-41.
22. Taylor AM, Rhee SW, Tu CH, Cribbs DH, Cotman CW, Jeon NL. Microfluidic multicompartment device for neuroscience research. Langmuir. 2003;19:1551-6.
23. Taylor AM, Blurton-Jones M, Rhee SW, Cribbs DH, Cotman CW, Jeon NL. A microfluidic culture platform for CNS axonal injury, regeneration and transport. Nature methods. 2005;2:599-605.
24. Claverol-Tinture E, Ghirardi M, Fiumara F, Rosell X, Cabestany J. Multielectrode arrays with elastomeric microstructured overlays for extracellular recordings from patterned neurons. J neural eng. 2005;2:L1-7.
25. Claverol-Tinture E, Cabestany J, Rosell X. Multisite recording of extracellular potentials produced by microchannel-confined neurons in-vitro. IEEE transactions on bio-medical engineering. 2007;54:331-5.
26. Pan L, Alagapan S, Franca E, Brewer GJ, Wheeler BC. Propagation of action potential activity in a predefined microtunnel neural network. J neural eng. 2011;8:046031.
27. Mangin JM, Gallo V. The curious case of NG2 cells: transient trend or game changer? ASN neuro. 2011;3:e00052.
28. Binczak S, Eilbeck JC, Scott AC. Ephaptic coupling of myelinated nerve fibers. Physica D: Nonlinear Phenomena. 2001;148:159-74.
29. Anastassiou CA, Perin R, Markram H, Koch C. Ephaptic coupling of cortical neurons. Nat Neurosci. 2011;14:217-23.
30. Katz B, Schmitt OH. Electric interaction between two adjacent nerve fibres. The Journal of Physiology. 1940;97:471-88.
31. Qiu C, Shivacharan RS, Zhang M, Durand DM. Can Neural Activity Propagate by Endogenous Electrical Field? The Journal of Neuroscience. 2015;35:15800-11.

APPENDIX

A.1 Extracting Spike height and width values.

In order to obtain spike points, spike height and spike width from the data given by SpyCode, this code is used. 'peak_train' contains all the sampling points where a spike exists. Spike height and width are represented by 'positive_spikes_voltage' and 'spikewidths'.

```
evoltage=full(peak_train);
pointsofspike= find(evoltage);
spike_time=pointsofspike/25000;
spike_height=full(peak_train(pointsofspike));
peak_train(7500001:end,:)=[1];
spike_voltage=data(pointsofspike);
test1=find(peak_train>0)
test2=find(data(test1)>0)
samplepoint_spike=test1(test2)
x=(1/25000:1/25000:length(data)/25000);

x1=x';
k=1;
positive_spikes_voltage=spike_voltage(find(spike_voltage>0));
positive_spikes_time=spike_time(find(spike_voltage>0));
positive_spikepoints=find(spike_voltage>0);
spike_height_positive=spike_height(find(spike_voltage>0));

width_cal_voltage=0.50*(positive_spikes_voltage);


  while k<=length(positive_spikes_time)
    p=samplepoint_spike(k);
     while p <= samplepoint_spike(k)

      if  data(p-1)<= width_cal_voltage(k) & data(p)>=width_cal_voltage(k)
      time_b_widthstart1(k)=x1(p-1);
      time_a_widthstart1(k)=x1(p);
      voltage_b_widthstart1(k)=data(p-1);
      voltage_a_widthstart1(k)=data(p);

      disp(time_b_widthstart1(k));
      disp(voltage_b_widthstart1(k));
      disp(time_a_widthstart1(k));
      disp(voltage_a_widthstart1(k));
      p=p-1;
      k=k+1;
```

```
        clear('p')
       break
        else
        p=p-1;
        end
       end
  end


time_b_widthstart=(time_b_widthstart1)';
time_a_widthstart=(time_a_widthstart1)';
voltage_b_widthstart=voltage_b_widthstart1';
voltage_a_widthstart=voltage_a_widthstart1';

x1=x';
n=1;

  while n<=length(positive_spikes_time)
     q=samplepoint_spike(n);
      while q <= 7500000

       if ( data(q)< width_cal_voltage(n) & data(q-1)>width_cal_voltage(n))
       time_b_widthstop1(n)=x1(q-1);
       time_a_widthstop1(n)=x1(q);
       voltage_b_widthstop1(n)=data(q-1);
       voltage_a_widthstop1(n)=data(q);

       disp(time_b_widthstop1(n));
       disp(voltage_b_widthstop1(n));
       disp(time_a_widthstop1(n));
       disp(voltage_a_widthstop1(n));
       q=q+1;
       n=n+1;
       break
       else
       q=q+1;
       end
      end
   end

time_b_widthstop=(time_b_widthstop1)';
time_a_widthstop=(time_a_widthstop1)';
voltage_b_widthstop=voltage_b_widthstop1';
voltage_a_widthstop=voltage_a_widthstop1';
```

```
for k=1:1:(length(positive_spikes_time));
   slopestart1(k)= (voltage_a_widthstart(k)-
voltage_b_widthstart(k))/(time_a_widthstart(k)-time_b_widthstart(k));
end

   slopestart=slopestart1';

for h=1:1:(length(positive_spikes_time));
widthstart1(h)=((slopestart(h).*time_a_widthstart(h))-
voltage_a_widthstart(h)+width_cal_voltage(h))/slopestart(h);
  end

widthstart=widthstart1';

for j=1:1:(length(positive_spikes_time));
   slopestop1(j)= (voltage_a_widthstop(j)-voltage_b_widthstop(j))/(time_a_widthstop(j)-
time_b_widthstop(j));
end

   slopestop=slopestop1';

for m=1:1:(length(positive_spikes_time));
widthstop1(m)=((slopestop(m).*time_a_widthstop(m))-
voltage_a_widthstop(m)+width_cal_voltage(m))/slopestop(m);
end

widthstop=widthstop1';

spikewidths=(widthstop-widthstart)*1000;
errornegative=find(spikewidths<0);
positive_spikes_time1=positive_spikes_time;
positive_spikes_voltage1=positive_spikes_voltage;
spikewidths1=spikewidths;

%Code below tags and removes the tail end of the spikes
error_tail1=[1];
qq=2;rr=1;
while qq<=length(positive_spikes_time)
  while rr<= length(positive_spikes_time)
if (positive_spikes_time(qq)-positive_spikes_time(qq-1)<=0.0032) &
(positive_spikes_voltage(qq))<(0.7*positive_spikes_voltage(qq-1))
error_tail1(rr)=qq;
rr=rr+1;
qq=qq+1;
break
else
```

```
   qq=qq+1;
   break
end
  end
end

error_tail=error_tail1';
positive_spikes_time(error_tail)=[1];
positive_spikes_voltage(error_tail)=[];
spikewidths(error_tail)=[];
spike_height_positive(error_tail)=[];
%-------------------------------------------------------------------

sem=(std(spikewidths)/sqrt(length(spikewidths)));
mean1=mean(spikewidths);
std1=std(spikewidths);
deadtimems=1.6;
coefficientofvariation=std1/mean1;

hist(spikewidths,0:0.04:3);
[counts1,centers1] = hist(spikewidths,0:0.04:3);
counts=counts1'; centers=centers1';
 [r,c] = find(counts==max(counts(:)));
mode=centers(r);
hold on
xlabel('spikewidths in ms','FontSize', 30);
ylabel('Counts','FontSize', 30);
xlim([0 3])
title({['5 um tunnel'];['Electrode#25, 12 Days, Positive Spikes'];['Deadtime- ',
num2str(deadtimems)];['Spikes detected- ',num2str(length(spikewidths)), ', mean=
',num2str(roundsd((mean1),3))];['Standard Deviation= ', num2str(roundsd((std1),2)), ',
SEM= ', num2str(roundsd(sem,2)),', Coefficient of Variation= ',
num2str(roundsd(coefficientofvariation,2))]});
set(findall(gcf,'-property','FontSize'),'FontSize',20)
hold off

disp('SAVING Positive Section')
filename2='\\BREWERSERVER\Shared\udit\spike analysis january 2016\spike analysis
2016\width\positive\5um 12d (1507015) 150727\spikewidths 5um e25 tunnels.fig';
savefig(filename2);

filename='\\BREWERSERVER\Shared\udit\spike analysis january 2016\workspace
2016\width\positive\5um 12d (1507015) 150727\spikewidths 5um e25 tunnels.mat';
save(filename);
```

```
filename3='\\BREWERSERVER\Shared\udit\spike analysis january 2016\workspace 2016\Relevant\10um 20d (150715) 150804\e25.mat';
save(filename3,'positive_spikes_time','positive_spikes_voltage','spike_height_positive','spike_time','spikewidths')
```

A.2 In order to represent spike height and width variation in terms of clusters, the following code is used. 'data1' contains spike height and width measures.

```
[IDX,C,sumd,D]=kmedoids(data1(:,1:2),3); % The cluster number can be varied from here

 [counts1,centers1]=hist((IDX),1:1:3)
 counts=counts1';
 centers=centers1';

hold on
k=1;
r=1;
while r<=counts(1,:)
while k<=length(data1(:,1))

   if ((IDX(k))) ==1
     c1(r,:)=[data1(k,1),data1(k,2),data1(k,3)];
     k=k+1;
     r=r+1;

   else

     k=k+1;

end
end
end
plot(c1(:,1),c1(:,2),'mo')
clear('k'); clear('r');
ca=[10.^c1(:,1),10.^c1(:,2),c1(:,3)];

hold on
k=1;
r=1;
while r<=counts(2,:)
while k<=length(data1(:,1))

   if ((IDX(k))) ==2
```

```
      c2(r,:)=[data1(k,1),data1(k,2),data1(k,3)];
      k=k+1;
     r=r+1;

    else

   k=k+1;

  end
end
end
plot(c2(:,1),c2(:,2),'ro')
clear('k'); clear('r');
cb=[10.^c2(:,1),10.^c2(:,2),c2(:,3)];

hold on
k=1;
r=1;
while r<=counts(3,:)
while k<=length(data1(:,1))

   if ((IDX(k))) ==3
      c3(r,:)=[data1(k,1),data1(k,2),data1(k,3)];
      k=k+1;
      r=r+1;

   else

    k=k+1;

   end
end
end
plot(c3(:,1),c3(:,2),'yo')
clear('k'); clear('r');
cc=[10.^c3(:,1),10.^c3(:,2),c3(:,3)];


xlabel('Log10(Spike Height (uV))')
ylabel('Log10(Spike Width (ms))')
xlim([0.7 2.7])
ylim([-1 0.6])

set(findall(gcf,'-property','FontSize'),'FontSize',20)
legend('C1','C2','C3')
```

A.3 Waveforms of clusters obtained from kmedoid function in A2 are aligned using this code. 'ca(:,3)','cb (:,3)','cc (:,3)' contains the timing of each spike in different clusters.

```
c1_time=ca(:,3)
samplingpoint_c1_time(:,2)=25000.*c1_time;
samplingpoint_c1_time(:,1)=samplingpoint_c1_time(:,2)-125;
samplingpoint_c1_time(:,3)=samplingpoint_c1_time(:,2)+125;

c2_time=cb(:,3)
samplingpoint_c2_time(:,2)=25000.*c2_time;
samplingpoint_c2_time(:,1)=samplingpoint_c2_time(:,2)-125;
samplingpoint_c2_time(:,3)=samplingpoint_c2_time(:,2)+125;

c3_time=cc(:,3)
samplingpoint_c3_time(:,2)=25000.*c3_time;
samplingpoint_c3_time(:,1)=samplingpoint_c3_time(:,2)-125;
samplingpoint_c3_time(:,3)=samplingpoint_c3_time(:,2)+125;

hold on

i=1;
for i=1:length(samplingpoint_c1_time(:,3))
time_spike_range(:,i)=[samplingpoint_c1_time(2,1)/25000:1/25000:samplingpoint_c1_tim
e(2,3)/25000];
end
j=1;
for j=1:length(samplingpoint_c1_time(:,3))
voltage_spike_range(:,j)=data(samplingpoint_c1_time(j,1):samplingpoint_c1_time(j,3));
end

k=1
for k=1:100 % First 100 spikes
   plot(time_spike_range(:,k),voltage_spike_range(:,k),'m');
hold on
end

xlabel('Spike Time (ms)')
ylabel('Spike Height (uV)')
set(findall(gcf,'-property','FontSize'),'FontSize',20)
hold on


i=1;
for i=1:length(samplingpoint_c1_time(:,3))
```

```
time_spike_range(:,i)=[samplingpoint_c1_time(2,1)/25000:1/25000:samplingpoint_c1_tim
e(2,3)/25000];
end
j=1;
for j=1:length(samplingpoint_c2_time(:,3))
voltage_spike_range(:,j)=data(samplingpoint_c2_time(j,1):samplingpoint_c2_time(j,3));
end

k=1
for k=1:100 % First 100 spikes
   plot(time_spike_range(:,k),voltage_spike_range(:,k),'r');
hold on
end

xlabel('Spike Time (ms)')
ylabel('Spike Height (uV)')
set(findall(gcf,'-property','FontSize'),'FontSize',20)

hold on

i=1;
for i=1:length(samplingpoint_c1_time(:,3))
time_spike_range(:,i)=[samplingpoint_c1_time(2,1)/25000:1/25000:samplingpoint_c1_tim
e(2,3)/25000];
end
j=1;
for j=1:length(samplingpoint_c3_time(:,3))
voltage_spike_range(:,j)=data(samplingpoint_c3_time(j,1):samplingpoint_c3_time(j,3));
end

k=1
for k=1:100 % First 100 spikes
   plot(time_spike_range(:,k),voltage_spike_range(:,k),'y');
hold on
end

xlabel('Spike Time (ms)')
ylabel('Spike Height (uV)')
set(findall(gcf,'-property','FontSize'),'FontSize',20)
```